Applied Physics A (2020) 126:252
https://doi.org/10.1007/s00339-020-3410-2

Applied Physics A
Materials Science & Processing

S.I. : CURRENT STATE-OF-THE-ART IN LASER ABLATION

Study on nonthermal–thermal processing boundary in drilling of ceramics using ultrashort pulse laser system with variable parameters over a wide range

Aiko Narazaki[1] · Hideyuki Takada[1] · Dai Yoshitomi[1] · Kenji Torizuka[1] · Yohei Kobayashi[2]

Received: 15 October 2019 / Accepted: 17 February 2020 / Published online: 4 March 2020

Abstract
Quality and throughput of laser material processing are influenced by multiple laser parameters as well as material properties. Since material degradation due to laser processing is generally related to heat-affected zone, quick optimization and realization of nonthermal process is one of the most important issues for higher-grade laser processing. In this work, we developed various parameter-controlled ultrashort pulse laser system that can control various laser parameters over a wide range, such as pulse duration over three orders of magnitude. Using this laser system (wavelength: 1033 nm, pulse duration: 0.4 to 400 ps, repetition: up to 1 MHz), we have investigated nonthermal–thermal processing boundary in drilling of ceramics: aluminum nitride (AlN) and yttria-stabilized zirconia (YSZ), with high and low thermal conductivity, respectively. As a result, the AlN ceramic exhibited strong dependence of ablation rate on fluence: low-, mid- and high-fluence regimes appeared with different logarithmic correlations. Further, the nonthermal–thermal process boundaries appeared, depending on the pulse duration. On the other hand, the ablation behavior of YSZ was much different from AlN; the ablation rate did not show distinct three regimes. Further, there were no nonthermal process windows for the YSZ. Therefore, the nonthermal–thermal process boundaries were governed by the laser parameters like pulse duration as well as the material thermal conductivity.

Keywords Ultrashort pulse laser · Drilling · Ceramics

1 Introduction

Ultrashort pulse laser processing has been attracting considerable attention due to its effectiveness for precise microfabrication and surface modification [1–10]. Consequently, there is growing industrial interest in ultrashort pulse lasers as powerful manufacturing tools for modern microfabrication, including in the automotive, aerospace, electro-optics, photonics, biomedical, semiconductors industries. For the industrial applications, this technology needs laser sources with higher average power that generate more pulses per time (higher repetition rate) and/or higher pulse energies [11–16]. High average power lasers accelerate the ablation process but also cause new problems, namely thermal damages owing to single-pulse-induced thermal damages and heat accumulation under multi-pulse irradiation. Thus, quick optimization and realization of nonthermal processes is an important issue for higher-grade laser processing [10]. However, there have been few systematic reports on the influence of laser and material parameters on the nonthermal–thermal processing boundary. In particular, the effect of laser pulse duration on such boundary is important but scarce because it is still difficult to change laser pulse duration over a wide range without changing other laser parameters. In order to break through such situations, we recently developed a 100-W average power femtosecond fiber laser system with variable parameters, which is capable of changing laser parameters in a wide range, such as the pulse duration over three orders of magnitude from 0.4 to 400 ps [17].

Ceramics have excellent heat resistance, corrosion resistance and electrical insulation and are active in various fields such as semiconductors, automobiles, information communication, industrial machinery, medical care, and so forth.

✉ Aiko Narazaki
narazaki-aiko@aist.go.jp

[1] Electronoics and Photonics Research Institute, National Institute of Advanced Industrial Science and Technology (AIST), Central 2, 1-1-1 Umezono, Tsukuba, Ibaraki 305-8568, Japan

[2] The Institute for Solid State Physics, The University of Tokyo, 5-1-5 Kashiwanoha, Kashiwa 277-8581, Japan

They are so hard and brittle that there is a great need for the laser processing of ceramics [6, 18–20]. Other attractive feature of ceramics is able to control thermal conductivity to various values, which might be one of the most important material parameters related to the laser processing quality. For example, there is a difference of about two orders of magnitude between aluminum nitride (AlN) with the higher thermal conductivity and yttria-stabilized zirconia (YSZ) with the lower one. The AlN ceramic is a material with high electrical insulation properties, good thermal conductivity with more than 230 W m^{-1} K^{-1} and a linear expansion coefficient close to Si and high chemical resistance and is widely used as heat dissipation substrates and components for semiconductor manufacturing equipment. On the other hand, YSZ has the highest strength and toughness among ceramics and is used for cutting tools. Since the thermal conductivity is about 3 W m^{-1} K^{-1}, much smaller compared to other ceramics, a high heat insulation effect can be expected and used for thermal barrier coating. Further, the application of YSZ expands to biomedical fields due to both the high strength and excellent stability even in human body.

In this work, we investigated nonthermal–thermal processing boundaries in laser micro-drilling of AlN and YSZ ceramics using our ultrashort pulse laser system with variable parameters over a wide range. The boundary separates the nonthermal and thermal process conditions; the former can realize the laser processing without heat damages, and the latter is accompanied by significant melt formation. We conducted the laser percussion micro-drilling of the ceramics at a pulse duration of 0.4 to 200 ps. As a result, we found the existence of nonthermal–thermal processing boundaries in the case of AlN, whereas there were no boundaries for YSZ. Even in the case of AlN, the nonthermal process window noticeably varied with the pulse duration.

2 Experimental details

Laser percussion drilling of AlN and YSZ ceramics was conducted using in-house developed ultrashort pulse laser system, which is capable of varying several parameters over a wide range. We developed an Yb-doped fiber chirped-pulse amplification system operated at a wavelength of 1033 nm and a maximum power of over 100 W [17], as shown in Fig. 1. The pulse duration can be controlled from 0.4 to 400 ps using a 300-mm-wide dielectric-coated grating with a groove density of 1740 lines/mm. The pulse repetition rate can be set to an arbitrary fractional frequency of 1 MHz. In this work, the pulse repetition rate was fixed at a maximum value of 1 MHz, which is suitable for higher productivity. The linearly polarized Gaussian beam was focused through a lens with a focal length of 100 mm on sample surfaces to a spot size of about 42 µm ($1/e^2$ diameter) in air.

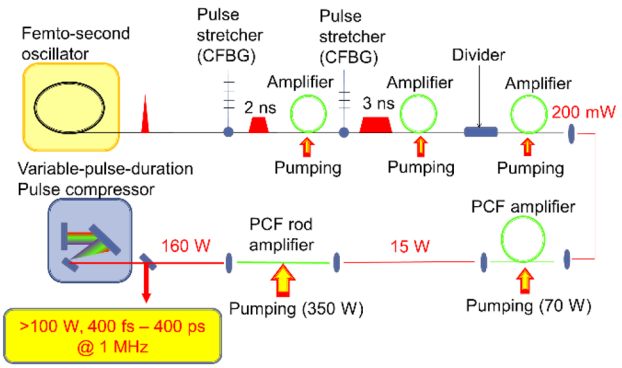

Fig. 1 Schematic diagram of a ultrashort pulse laser system that can change various parameters over a wide range

AlN ceramic plates (Furukawa denshi) with a thermal conductivity of 170–230 W m^{-1} K^{-1} were used as samples in this work. The sample thickness was about 500 µm or 1 mm. YSZ (Nishimura advanced ceramics, 3 mol% of yttria) ceramic plates have a thermal conductivity of approximately 3 W m^{-1} K^{-1}, which is two orders of magnitude smaller than that for the AlN ceramic.

The whole images of drilled micro-holes on the AlN and YSZ ceramics as well as the ablation volume were obtained by the confocal laser scanning microscope (Olympus, OSL4000). For quality analysis, the surface and cross-sectional morphology were observed in detail using a field emission–scanning electron microscope (FE-SEM; Hitachi S-4800). The cross-sectional SEM observation of the drilled micro-holes was realized by polishing using SiC abrasive paper after mechanical cutting in the vicinity of the hole. The chemical composition in the drilled holes was analyzed by an energy-dispersive X-ray spectrometer (EDX; Horiba EMAX) attached to the FE-SEM.

3 Results and discussion

3.1 Influence of pulse duration and fluence on ablation volume

First, the influence of basic laser parameters like pulse duration, τ_p, and fluence, F, on ablation volume was investigated. Figure 2a is a 2D array of confocal laser scanning microscopic images of holes on the AlN ceramic as a function of the pulse duration and peak fluence. The number of pulses, N_p, was fixed at 100. The AlN ablation began with a fluence of about 0.5 J cm^{-2}, and there was no significant dependence on the pulse duration. At $\tau_p = 0.4$ ps, the average hole diameter at a sample surface increased from about 33 µm at 0.6 J cm^{-2} to 55 µm at 7 J cm^{-2}. The ablation volume corresponding to the images in Fig. 2a was calculated from

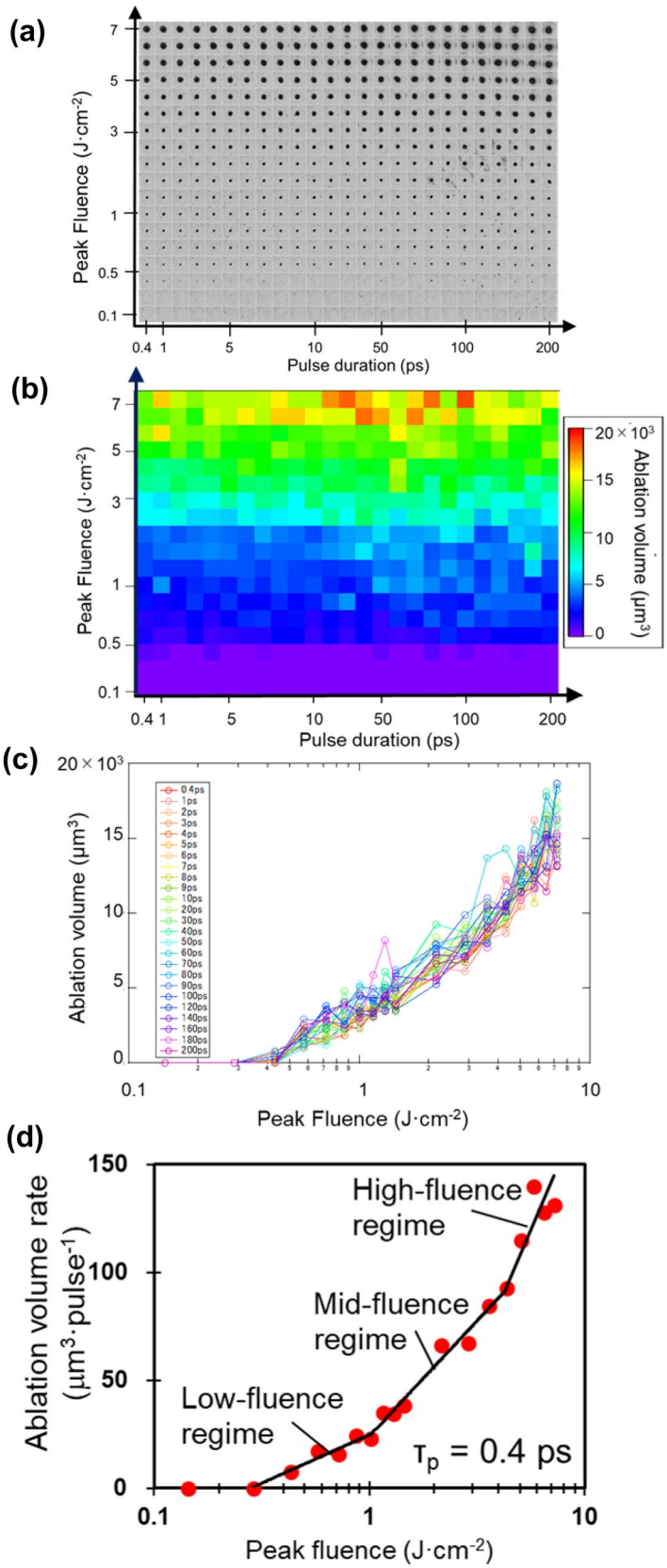

Fig. 2 **a** Confocal laser scanning microscopic images and **b** the ablation volume of holes percussion drilled on AlN ceramic are presented as a function of the pulse duration, τ_p, and the peak fluence. **c** The ablation volume versus the peak fluence at different pulse durations; N_p was set at 100. **d** The ablation volume rate as a function of peak fluence at $\tau_p = 0.4$ ps

the confocal laser scanning microscopic measurements and is plotted in Fig. 2b. Similar to Fig. 2a, there was no obvious dependence of the ablation volume on pulse duration. Figure 2c plots the ablation volume versus the peak fluence at different pulse durations. The ablation volume rose with an increase in fluence. In order to take a closer look, the ablation volume rate at $\tau_p = 0.4$ ps is plotted against the peak fluence in Fig. 2d. As a result, three types of ablation regimes that have different logarithmic correlations between the ablation volume and fluence appeared. The appearance of two or three regimes has been reported for metals such as copper and stainless steel [21, 22]. The low- and high-fluence regimes correspond to different energy transport mechanisms; in the former regime, the ablation is governed by optical penetration of laser beam, whereas in the latter regime, heat transport thermally driven by electrons becomes dominant. Thus, the latter leads to higher ablation rate, but easily degrades the surface quality due to melt formation. The third regime was sometimes observed between the low- and high-fluence regimes, namely mid-fluence regime, where high throughput and surface quality possibly coexist. It is noteworthy that the AlN has a thermal conductivity between copper (400 W m^{-1} K^{-1}) and stainless steel (15–30 W m^{-1} K^{-1}) and both the copper and stainless steel exhibited the three regimes. However, in the case of the AlN ceramic, the laser ablation mainly stems from multi-photon absorption at a laser wavelength of 1033 nm because the AlN is a material with wide band gap of about 6 eV, which is different from metals. Anyway, to our knowledge, this is the first report on the appearance of such three regimes for the ceramic material, although further investigation on the multi-regime origin is necessary.

Next, the same analyses were performed on YSZ ceramic as shown in Fig. 3. The hole diameter increased from about 25 µm at 1 J cm^{-2} to 50 µm at 7 J cm^{-2} at $\tau_p = 0.4$ ps. Different from AlN, the dependence of the ablation volume on the pulse duration was clearly observed. First, the shorter pulse duration exhibited the lower ablation threshold. For example, the ablated holes were observable at 1 J cm^{-2} or higher fluences in the case of $\tau_p = 0.4$ ps, while the hole began to be visible around 3 J cm^{-2} for $\tau_p = 200$ ps. Therefore, the ablation threshold is reduced to one-third by reducing the pulse duration from 200 ps to 0.4 ps. Second, the behavior of ablation volume rate with respect to fluence varies depending on the pulse duration as shown in Fig. 3d. At shorter pulse duration of 0.4 ps, the ablation volume rate increased logarithmically with the fluence up to below 4 J cm^{-2}. Then, it started a sudden rise and finally peaked around 6 J cm^{-2}. On the other hand, at longer pulse duration of 200 ps, the ablation volume rate drastically increased above the ablation threshold, resulting in larger ablation volume. This high ablation regime was accompanied with heavy melt formation and splashing, and it was not a stable process.

Anyway, it became clear that the dependence of ablation on laser parameters like the pulse duration and fluence differs greatly between AlN and YSZ ceramics.

3.2 Influence of laser and material parameters on ablation quality

In order to investigate the effects of laser and material parameters on laser processing quality, especially surface features, FE-SEM observation of laser processed holes was performed. Figure 4 shows SEM images of micro-holes on AlN ceramic drilled at different laser pulse durations of (a) 0.4 ps, (b) 1 ps, (c) 10 ps, (d) 100 ps and (e) 200 ps, respectively. The F and N_p were set at 7 J cm^{-2} and 100. The center and right-hand column images were obtained by high-magnification observation at the center and edge of the holes. For $\tau_p = 0.4$ ps, at the center of the hole bottom, laser-induced periodic surface structures (LIPSS) were observed with direction perpendicular to laser linear polarization and periodicity of about 1 µm less than and comparable to the laser wavelength, which the literature [9] called "ripple." This ripple at the center of the hole bottom was visible up to 10 ps while fading gradually. At 100 ps or more, the ripple disappears completely at the center of the hole bottom and was covered with a melt-solidified layer. On the other hand, at the edge of the hole, namely hole sidewall, the appearance of ripple structures was confirmed, which has a periodicity of about 350 nm (approximately 30% of the wavelength of the laser) and perpendicular to the laser polarization. The smaller ripple was clearly confirmed up to 100 ps, and there is no trace of melting materials at the hole sidewalls, as shown in Fig. 4a–d. At 200 ps, it started to be covered with a melt in Fig. 4e.

The formation of ripples may be attributed to the optical interference of an incident femtosecond laser irradiation with a surface scattered wave for silicon semiconductor [23]. Thus, such a nanostructured ripple formation can be attributed to a nonthermal phenomenon, which does not accompany drastic melt formation. At 200 ps, the hole surface has melted and re-solidified, as shown in Fig. 4e. However, ripples with sub-wavelength periods were partially observed under the melt-solidified layer. From these, the following model can be proposed. Initially, ripple structures are formed at the entire pulse duration range from 0.4 to 200 ps. Successive laser pulses incident on the same spot cause heat accumulation, thereby raising the temperature around the laser spot. When this exceeds a characteristic temperature, such as the equilibrium melting point, it results in melting around the laser irradiation spot. This model suggests that the effect of heat accumulation increases as the pulse duration increases, making it easier for the temperature to rise due to heat accumulation.

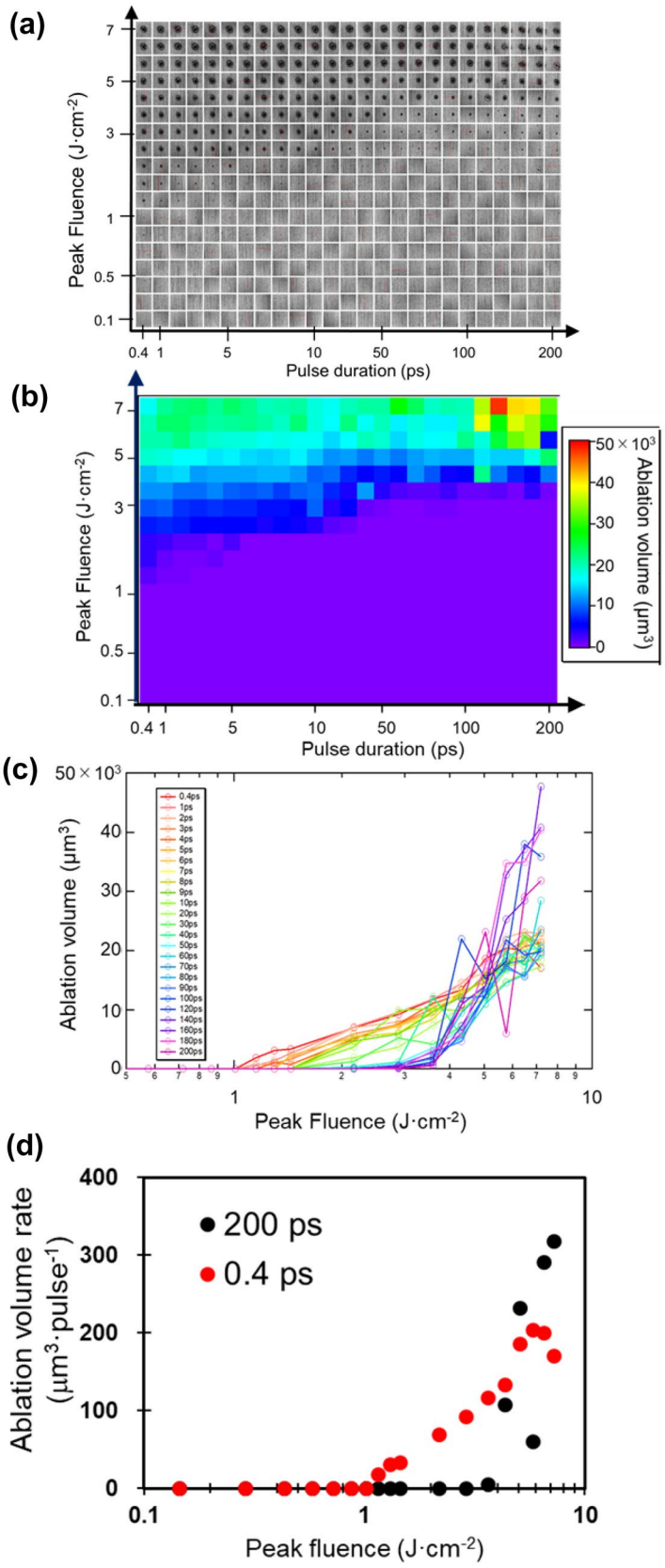

Fig. 3 **a** Confocal laser scanning microscopic images and **b** the ablation volume of holes percussion drilled on YSZ ceramic are presented as a function of the pulse duration and the peak fluence. **c** The ablation volume versus the peak fluence at different pulse durations ($N_p = 100$). **d** The ablation volume rate as a function of peak fluence at $\tau_p = 0.4$ ps (red circles) and 200 ps (black circles)

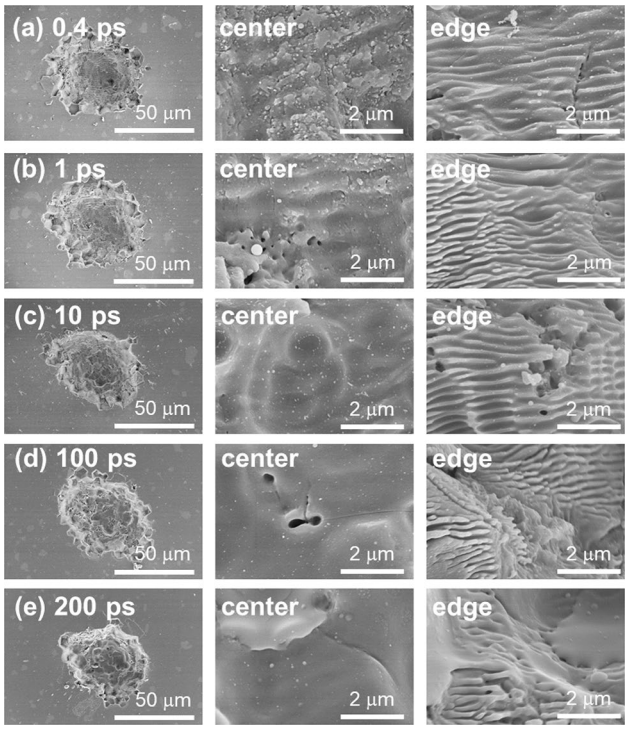

Fig. 4 SEM images of micro-holes on AlN ceramic drilled at different laser pulse durations of **a** 0.4 ps, **b** 1 ps, **c** 10 ps, **d** 100 ps and **e** 200 ps, respectively. The F and N_p were 7 J cm^{-2} and 100. The center and right images were obtained by high-magnification observation at the center and edge of the holes

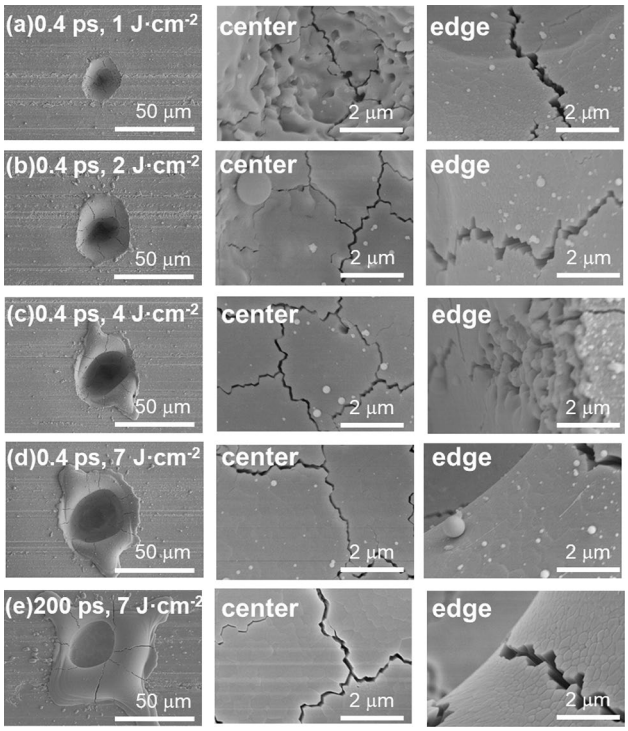

Fig. 5 SEM images of micro-holes on YSZ ceramic drilled at different peak fluences of **a** 1 J cm^{-2}, **b** 2 J cm^{-2}, **c** 4 J cm^{-2} and **d** 7 J cm^{-2}; τ_p and N_p were 0.4 ps and 100. The pulse duration was changed to 200 ps for the image **e** (F = 7 J cm^{-2}). The center and right images were obtained by high-magnification observation at the center and edge of the holes, respectively

Figure 5 shows SEM images of micro-holes on YSZ ceramic drilled at different peak fluences of (a) 1 J cm^{-2}, (b) 2 J cm^{-2}, (c) 4 J cm^{-2} and (d) 7 J cm^{-2}; τ_p and N_p were set at 0.4 ps and 100. The pulse duration was changed to 200 ps for the image (e) (F = 7 J cm^{-2}). The center and right images were obtained by high-magnification observation at the center and edge of the holes, respectively. In contrast to AlN ceramic, there was no ripple formation for YSZ ceramic even at the shortest pulse duration of 0.4 ps in this work. As shown in Fig. 5a–d, all holes have the same surface structures at the center and edge of holes; they have a smooth melt-solidified surface with many cracks. The only difference depending on the fluence is the rim formation around the hole; noticeable rim formation started at a fluence above 4 J cm^{-2}. This suggests that the ablation due to the removal of molten pool may begin to dominate, which corresponds to the fluence dependence of the ablation volume in Fig. 3d.

To examine the influence of pulse duration on the hole quality, the micro-holes prepared at τ_p = 0.4 and 200 ps are compared in Fig. 5d, e. In the case of 200 ps, the rim formation was seen in a wider area. Furthermore, Fig. 3c, d indicates that the longer pulse duration can remove larger volume. However, because the fluence dependence of the removal volume seems unstable, this removal process is not stable. These facts suggest that the ablation of YSZ ceramic with lower thermal conductivity tends to occur via thermal process with the formation and removal of a larger melt pool.

3.3 Nonthermal–thermal processing boundary for ceramics

Finally, we will discuss about nonthermal–thermal processing boundaries for AlN and YSZ ceramics in terms of the quality of processed holes based on FE-SEM observation. Figure 6a shows cross-sectional SEM images of AlN ceramic holes drilled by laser percussion irradiation with 10^3 (lower) and 10^7 (upper). The τ_p and F were set at 0.4 ps and 4 J cm^{-2}, respectively. The lower hole had a sidewall with a ripple structure, while the upper one had a smooth and cracked surface specific to melt solidification. Thus, the process, where holes with smooth and cracked sidewalls like the upper image in Fig. 6a were made, is defined as a "thermal" one. On the other hand, the process, where holes with other types of sidewalls such as a ripple in the lower image in Fig. 6a were formed, is referred to a "nonthermal" one.

Using the above definition, the thermal (red circles) and nonthermal (blue circles) process conditions for AlN

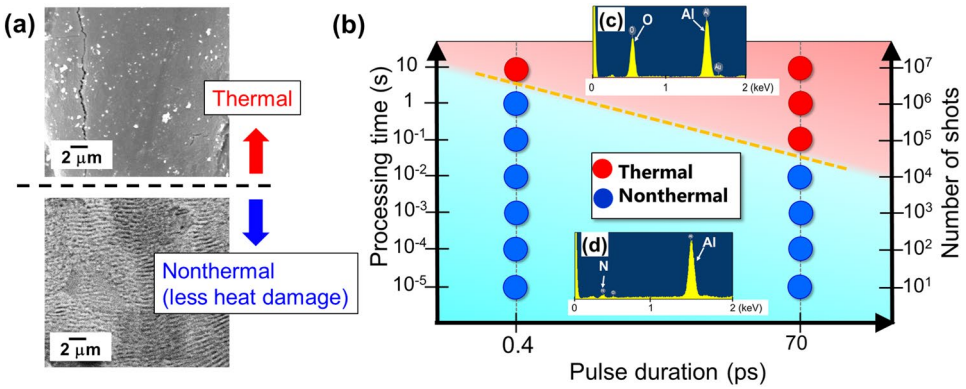

Fig. 6 **a** Cross-sectional SEM images of AlN ceramic holes drilled by laser percussion irradiation with 10^3 (lower) and 10^7 (upper). The τ_p and F were set at 0.4 ps and 4 J cm^{-2}. The lower hole had a sidewall with a typical ripple structure, while the upper one had a smooth surface after melt solidification. We defined the upper and lower surfaces as "thermal" and "nonthermal" processes because the ripple appeared in the case of less thermal damages. **b** Morphology dependence on pulse duration and number of pulses for drilling of AlN ceramics ($F=4$ J cm^{-2}). Red and blue circles represent the holes with the inner surfaces like the upper and lower surfaces in (**a**), namely obtained by the thermal and nonthermal processes. SEM–EDX spectra are also shown in (**c**) and (**d**) for $N_p=10^7$ and 10^3, respectively, at 0.4 ps

ceramic were plotted as a function of the pulse duration and number of pulses, namely processing time in Fig. 6b. As a result, it was found that boundaries between nonthermal and thermal processing appeared. Further, this boundary depends on the pulse duration; while the boundary existed between $N_p=10^6$ and 10^7 at 0.4 ps, it appeared between $N_p=10^4$ and 10^5 at 70 ps. This suggests that the shorter pulse duration enables the wider range of nonthermal processing conditions. That is, the shorter pulse duration might open wider nonthermal process windows. This might be related to the dependence of heat accumulation on the pulse duration. SEM–EDX spectra are also shown in Fig. 6c, d for $N_p=10^7$ and 10^3, respectively, at $\tau_p=0.4$ ps. In Fig. 6c for the melt-solidified inner wall obtained by the thermal process, there were two main peaks assigned to O and Al elements, indicating drastic oxidation during the laser drilling process. In contrast, the EDX spectrum from the inner wall with the ripple structure was similar to that of a pristine surface of AlN ceramic, indicating that there was no noticeable change in the chemical composition. Consequently, the nonthermal process is vital to keep the processed holes with less heat damages and no compositional changes for achieving higher-quality laser micro-drilling of AlN ceramics.

In the case of YSZ with lower thermal conductivity, there was no nonthermal processing window in an entire fluence range in this work, based on the above results in Fig. 5. Figure 7 shows the typical morphology dependence on pulse duration and number of pulses for YSZ ceramic ($F=7$ J cm^{-2}). For reference, SEM images of the micro-holes drilled at the pulse duration of (b) 0.4 ps, (c) 10 ps and (d) 200 ps are also shown in Fig. 7. Over the full fluence range in this work, holes with smooth and cracked surfaces were obtained as shown in Fig. 7b–d.

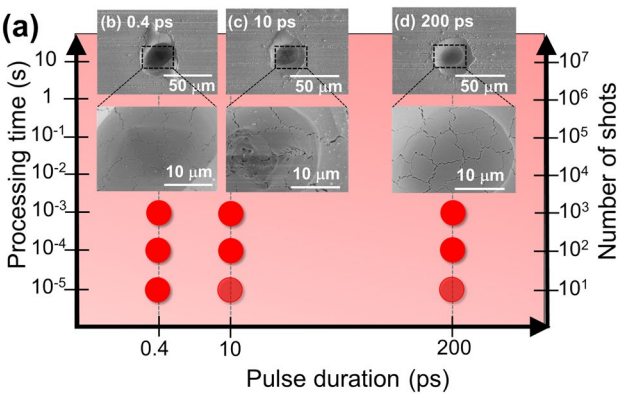

Fig. 7 **a** Morphology dependence on pulse duration and number of pulses for drilling of YSZ ceramic ($F=7$ J cm^{-2}). Red circles represent the holes with the melt-solidified inner wall like the upper surface in Fig. 6a, namely obtained by the thermal process. SEM images for the micro-holes drilled at the pulse duration of **b** 0.4 ps, **c** 10 ps and **d** 200 ps are also shown, respectively

Comparison of Fig. 4a for AlN and Fig. 5d for YSZ indicates that nonthermal and thermal processing is determined depending on materials even under exactly the same laser parameters. In this work, the nonthermal–thermal process boundaries were governed by both the laser parameters such as pulse duration and fluence and material properties such as thermal conductivity. In future, such a governing equation would be unveiled and used for quick process optimization toward the realization of both higher throughput and quality.

4 Summary

We developed ultrashort pulse laser system that can change a number of laser parameters over a wide range, such as the pulse duration over three orders of magnitude. Using the laser system, we have investigated nonthermal–thermal processing boundaries in laser drilling of AlN and YSZ ceramics with high and low thermal conductivity. The AlN ceramic exhibited the strong dependence of ablation rate on fluence; the ablation rate rose in three regimes which have different logarithmic correlations. It was also found that there were the nonthermal–thermal process boundaries, depending on the pulse duration. Different from AlN, YSZ did not show the above three regimes. Further, there was no nonthermal processing window in an entire fluence range for the YSZ. Therefore, it was found that the nonthermal–thermal process boundaries were mainly governed by both the pulse duration and material property such as thermal conductivity.

Acknowledgements This work was financially supported by the New Energy and Industrial Technology Development Organization (NEDO).

References

1. S. Preuss, E. Matthias, M. Stuke, Sub-picosecond UV-laser ablation of Ni films: strong fluence reduction and thickness-in-dependent removal. Appl. Phys. A **59**, 79–82 (1994)
2. B.N. Chichkov, C. Momma, S. Nolte, F. von Alvensleven, A. Tünnermann, Femtosecond, picosecond and nanosecond laser ablation of solids. Appl. Phys. A **63**, 109–115 (1996)
3. T.V. Kononenko, V.I. Konov, S.V. Garnov, R. Danielius, A. Piskarskas, G. Tamoshauskas, F. Dausinger, Comparative study of the ablation of materials by femtosecond and pico- or nanosecond laser pulses. Quantum Electron. **29**, 724–728 (1999)
4. M. Hashida, H. Mishima, S. Tokita, S. Sakabe, Non-thermal ablation of expanded polytetrafluoroethylene with an intense femtosecond-pulse laser. Opt. Express **17**, 13116–13121 (2009)
5. J. Byskov-Nielsen, J.M. Savolainen, M.S. Christensen, P. Balling, Ultra-short pulse laser ablation of copper, silver and tungsten: experimental data and two-temperature model simulations. Appl. Phys. A **103**, 447–453 (2011)
6. N. Ackerl, M. Warhanek, J. Gysel, K. Wegener, Ultrashort-pulsed laser machining of dental ceramic implants. J. Eur. Ceram. Soc. **39**, 1635–1641 (2019)
7. F. Korte, S. Adams, A. Egbert, C. Fallnich, A. Ostendorf, Sub-diffraction limited structuring of solid targets with femtosecond laser pulses. Opt. Express **7**, 41–49 (2000)
8. G. Miyaji, K. Miyazaki, Origin of periodicity in nanostructuring on thin film surfaces ablated with femtosecond laser pulses. Opt. Express **16**, 16265–16271 (2008)
9. G.D. Tsibidis, C. Fotakis, E. Stratakis, From ripples to spikes: a hydrodynamical mechanism to interpret femtosecond laser-induced self-assembled structures. Phys. Rev. B **92**, 041405 (2015)
10. A. Narazaki, J. Nishinaga, H. Takada, T. Sato, H. Niino, K. Torizuka, Y. Kamikawa-Shimizu, S. Ishizuka, H. Shibata, S. Niki, Evaluation of femtosecond laser-scribed Cu(In, Ga)Se2 solar cells using scanning spreading resistance microscopy. Appl. Phys. Express **11**, 032301 (2018)
11. J. Finger, M. Reininghaus, Effect of pulse to pulse interactions on ultrashort pulse laser drilling of steel with repetition rates up to 10 MHz. Opt. Express **22**, 18790–18799 (2014)
12. C. Kerse, H. Kalaycıoğlu, P. Elahi, B. Çetin, D.K. Kesim, Ö. Akçaalan, S. Yavaş, M.D. Aşık, B. Öktem, H. Hoogland, R. Holzwarth, F.Ö. Ilday, Ablation-cooled material removal with ultrafast bursts of pulses. Nature **537**, 84–88 (2016)
13. J. Mur, R. Petovsek, Near-THz bursts of pulses–Governing surface ablation mechanisms for laser material processing. Appl. Surf. Sci. **478**, 355–360 (2019)
14. R. Weber, T. Graf, P. Berger, V. Onuseit, M. Wiedenmann, C. Freitag, A. Feuer, Heat accumulation during pulsed laser materials processing. Opt. Express **22**, 11312–11324 (2014)
15. F. Bauer, A. Michalowski, T. Kiedrowski, S. Nolte, Heat accumulation in ultra-short pulsed scanning laser ablation of metals. Opt. Express **23**, 1035–1043 (2015)
16. A. Gruner, J. Schille, U. Loeschner, High repetition frequency micro hole drilling of metal foils using ultrashort pulse laser radiation. Proc. SPIE **10520**, 105200R (2018)
17. D. Yoshitomi, H. Takada, K. Torizuka, Y. Kobayashi, 100-W average-power femtosecond fiber laser system with variable parameters for rapid optimization of laser processing, in *Conference on Lasers and Electro-Optics OSA Technical Digest (Optical Society of America)*, paper SM3L.2 (2019)
18. Y. Hirayama, H. Yabe, M. Obara, Selective ablation of AlN ceramic using femtosecond, nanosecond, and microsecond pulsed laser. J. Appl. Phys. **89**, 2943–2949 (2001)
19. S.H. Kim, T. Balasubramani, I.B. Sohn, Y.C. Noh, J. Lee, S. Jeong, Precision microfabrication of AlN and Al_2O_3 ceramics by femtosecond laser ablation. Proc. SPIE **6879**, 68791 (2008)
20. V. Nasrollahi, P. Penchev, T. Jwad, S. Dimov, K. Kim, C. Im, Drilling of micron-scale high aspect ratio holes with ultra-short pulsed lasers: critical effects of focusing lenses and fluence on the resulting holes' morphology. Opt. Lasers Eng. **110**, 315–322 (2018)
21. S. Nolte, C. Momma, H. Jacobs, A. Tuennermann, B.N. Chichkov, B. Wellegehausen, H. Welling, Ablation of metals by ultrashort laser pulses. J. Opt. Soc. Am. B **14**, 2716–2722 (1997)
22. J. Schille, L. Schneider, U. Loeschner, Process optimization in high-average-power ultrashort pulse laser microfabrication: how laser process parameters influence efficiency, throughput and quality. Appl. Phys. A **120**, 847–855 (2015)
23. T.H.R. Crawford, H.K. Haugen, Sub-wavelength surface structures on silicon irradiated by femtosecond laser pulses at 1300 and 2100 nm wavelengths. Appl. Surf. Sci. **253**, 4970–4977 (2007)